ISSN: 1813-162X (Print) ; 2312-7589 (Online)

Tikrit Journal of Engineering Sciences

available online at: http://www.tj-es.com

Abdel-Rahman ZA, Zeyad A. Abdullah. Utilization of CO_2 in Flue Gas for Sodium Bicarbonate Production in a Bubble Column. *Tikrit Journal of Engineering Sciences* 2019; 26(2): 28-38.

Utilization of CO_2 in Flue Gas for Sodium Bicarbonate Production in a Bubble Column

Zaid A. Abdel-Rahman*
Zeyad A. Abdullah

Chemical Engineering Department,
College of Engineering,
Tikrit University,
Tikrit,
Iraq

***Keywords*:**

CO_2
utilization,
sodium bicarbonate,
bubble column

ARTICLE INFO

Article history:

Received: 30 Sep. 2018
Accepted: 25 Feb. 2019
Available online: 05 Apr. 2019

ABSTRACT

Utilization of CO_2 in flue gases for the production of sodium bicarbonate is an environmentally friendly process. A mathematical model was constructed for the design and simulation of utilizing a low concentration CO_2 (2-18%) in flue gas to produce sodium bicarbonate in a bubble column reactor. The model is based on the mass balance equations for three phases (gas, liquid, and solid). Danckwerts theory for mass transfer from the gas phase to the liquid phase coupling with chemical reaction, and crystallization mechanism was used. The effect of process variables; gas molar velocity or flux (G=2.5-10 mole/m^2.s), liquid mass flow rate (m_L=2800-3400 kg/h), sodium bicarbonate concentration (x_1=0.04-0.1), CO_2 gas mole fraction (y=0.02-0.18), column height (h=11-33 m), and column diameter (d_R=1-3 m) on the objective variables; solid molar velocity (S), CO_2 conversion, precipitation zone height (Z_i), and crystal size distribution (CSD) were studied. The conversion of CO_2 varied from 34% to 71% whereas the particle size range varied from 0 to 400 µm**.** The particle size range and the CO_2 absorption efficiency of about 50% for 20 m column height are in agreement with the literature.

DOI: http://dx.doi.org/10.25130/tjes.26.2.05

استخدام ثاني اوكسيد الكاربون في غازات المداخن لانتاج بيكاربونات الصوديوم في عمود الفقاعات

الخلاصة

استخدم ثاني اوكسيد الكاربون في غازات المداخن لإنتاج بيكاربونات الصوديوم عملية صديقة للبيئة. تم بناء نموذج رياضي ومحاكاة لاستخدم تركيز واطئ (2-18%) ثاني اوكسيد الكاربون في غازات المداخن لإنتاج بيكاربونات الصوديوم في مفاعل عمود الفقاعات. استند الموديل على معادلات موازنة الكتلة للاطوار الثلاثة (غاز وسائل وصلب). واستعملت نظرية (Danckwerts) لانتقال الكتلة من الطور الغازي الى الطور السائل مع تفاعل كيميائي والية التبلور. وتم دراسة تأثير متغيرات العملية ؛ سرعة تدفق الغاز المولية (G=2.5-10 mole/m^2.s) ، معدل تدفق كتلة السائل (m_L=2800-3400 kg/h) ، تركيز بيكاربونات الصوديوم (x_1=0.04-0.1) ، والنسبة المولية لغاز ثاني اوكسيد الكاربون (y=0.02-0.18) ، ارتفاع العمود (h=11-33 m) ، وقطر العمود (d_R=1-3 m) على المتغيرات المستهدفة؛ معدل سرعة الصلب المولية(S) ، نسبة تحول غاز ثاني اوكسيد الكاربون ، ارتفاع منطقة الترسيب (Z_i) ، وتوزيع الحجم البلوري (CSD). كان التغير في نسبة تحول ثاني اوكسيد الكاربون من 34% الى 71% والحجم الحبيبي من 0 الى 400 مايكرون. وكانت حدود الحجم الحبيبي، وكفاءة امتصاص ثاني اوكسيد الكاربون بحدود 50% لارتفاع العمود 20 م متوافقة مع الادبيات المنشورة.

* Corresponding Author: E-mail: zaid572010@yahoo.com

1. INTRODUCTION

The decrease of carbon dioxide CO_2 emissions is vital to avoid the environmental problems. CO_2 conversion and utilization can play a significant role in reducing emissions. Appropriate chemical process can add an economic value to the CO_2 disposal by produce an industrially useful products. Sodium bicarbonate production is an environmentally friendly process [1].

The following equilibrium chemical reactions are occurring [2-3]:

$Na_2CO_3 \leftrightarrow 2Na^+ + CO3^{-2}$ (1)

$CO_2\ (g) \leftrightarrow CO_2\ (l)$ (2)

$CO_2\ (l) + OH^- \leftrightarrow HCO_3^-$ (3)

$CO_3^{-2} + H_2O \leftrightarrow HCO_3^- + OH^-$ (4)

$Na^+ + 2HCO_3^- \leftrightarrow 2NaHCO_3$ (5)

The overall chemical reaction is:

$Na_2CO_3 + CO_2 + H_2O \leftrightarrow 2NaHCO_3$ (6)

A bubble column reactor was used because of its important benefits which are: efficient heat and mass transfer, adequate operating conditions, low cost for operation and maintenance, and fixed parts leading to minimize the wear and tear [4].

Initially a supersaturated solution of NaHCO3 that formed according to the reaction equation (Eq.6) and then sodium bicarbonate crystals will be produced. The supersaturation is a governing driving force for the kinetics of the crystallization process. Supersaturated solution is not at equilibrium and the crystals is formed in its (nucleation stage) by various mechanisms mainly included primary nucleation in the non-existence of crystals and secondary nucleation in the existence of crystals. After that the volume of crystals is grown (growth stage). Optimal supersaturation is vital for economic production of the crystals with the required purity, size, and shape. The average size and crystal size distribution is affected by the crystallization kinetic and operating conditions [5,6].

Mathematical modeling of the bubble column reactors has always a significant role in reducing the experimental hard work that required for improving these devices in the industrial plants. Mathematical modeling and numerical simulation of such reactors (bubble column reactors) are increased and developed and constitutes an important path for giving a better understanding of processes and complex physical phenomena take place in bubble column reactors [7-8].

Two main groups of researchers studied the process of producing the sodium bicarbonate. They used pure or high CO_2 gas mole fraction (>50 %) in an industrial bubble column. The first researchers group used an industrial bubble column called (BIR) column (2.5 m diameter and 20 m height) with a circulation loops in the lower part of the column that providing a perfect mixing, the group is named as SOLVAY mixed flow group [9-14]. The second group used a plug flow industrial bubble column (1.2 m diameter and 22 m height) that located in Shiraz Petrochemical Complex in Iran and the group is named as SHIRAZ plug flow group [5,15-18].

Wylock et al [19] carried out an experimental analysis and the mathematical modeling of the CO_2 absorption in an aqueous solution of $NaHCO_3$ and Na_2CO_3 inside a Hele-Shaw cell. The absorption, driven by the combining diffusion and chemical reactions, eventually leads to the apparition of a peculiar gravitational instability or buoyancy-induced instability.

There are many unclear points in the previous mathematical model of SHIRAZ group. The typical operating conditions are not satisfying the mentioned productivity of $NaHCO_3$ (20,000 ton/y or 8.35 mole/m^2.s) according to the stoichiometric of chemical equation Eq. 6. The $NaHCO_3$ productivity of 8.35 (mole/m^2.s) could be obtained at inlet gas flow rate (Q_g) of 1500 Nm^3/h (15 mole/m^2.s), inlet liquid mass flow rate (m_L) of 7000 kg/h (66 mole/m^2.s), and Na_2CO_3 concentration (x_2) of 25% compared with 200 Nm^3/h (2 mole/m^2.s), 4800 kg/h (52 mole/m^2.s), 12% respectively. Also the CO_2 conversion trend does not express the normal behavior of the bubble column reactor because half of the height column appeared useless.

Few of the previous researches are existed for utilizing flue gas carbon dioxide in the production of sodium bicarbonate. In the present work, carbon dioxide in flue gas (at low concentration) was utilized in the production process of sodium bicarbonate.

The objectives of this study are to construct a suitable mathematical model for the design and simulation of utilizing low concentration CO_2 (2-18%) that is present in flue gas to produce sodium bicarbonate in bubble column reactor, to validate the model with literature data, and to study the effect of the process operating variables on the performance of the bubble column reactor.

2. MATHEMATICAL MODEL

The mathematical model is useful for the process design and simulation to obtain the optimal operations without changing the actual process.

The present mathematical model for bubble column for producing $NaHCO_3$ is constructed on the base of the equations of mass balance for three phases (gas, liquid, and solid), Danckwerts theory for mass transfer from the gas phase to the liquid phase coupling with chemical reaction, and solid crystallization involving crystals nucleation and growth. A plug flow one-dimensional control volume is considered along the length of column as shown in Fig. 1. The reactor is divided into two sections. The first section started from the top point of the reactor(z=h) to the point Z_i at which $NaHCO_3$ represents maximum supersaturation state and precipitation start, and the second section is started from the point Z_i to the bottom of column.

Many assumptions are considered in the model;

1- Steady state.
2- Uniform radial distribution.
3- Constant temperature.
4- Constant physical properties.

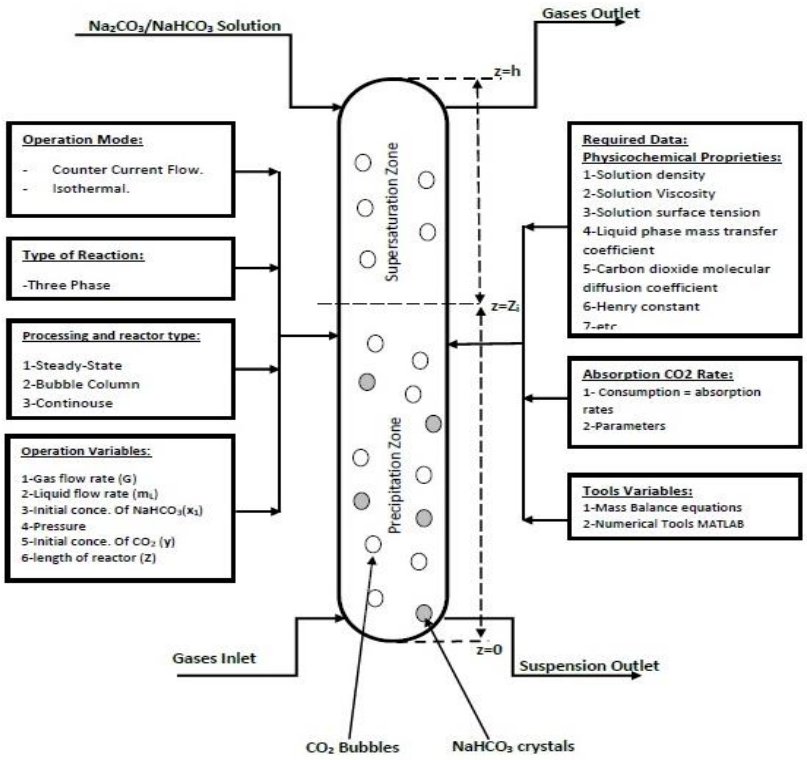

Fig. 1. Bubble column required data and tools for modeling and simulation

2.1 Mole Balance of Gas Phase

The mole balance equation of the gas phase (CO_2+Air) $(CO_2 + Air)$ around a differential element is:

$$\frac{dG}{dz} = -N_{CO_2}.\alpha_g \qquad (7)$$

Carbon dioxide absorbance rate was obtained by using the investigation of mass transfer with chemical reaction that given by Danckwerts and Lannus [20], using the following equation:

$$N_{CO_2} = E.H.K_L.\left(P_{CO_2} - P_{CO_{2\,e}}\right).\alpha_g \qquad (8)$$

The gas-liquid interface (α_g) is calculated by [21] ;

$$\alpha_g = 6\,\frac{\varepsilon_g}{d_b} \qquad (9)$$

The gas hold-up (ε_g) is calculated by [22] ;

$$\varepsilon_g = \frac{1}{2 + ((0.35/U_g)\,(\rho_l \sigma/72))^{\frac{1}{3}}} \qquad (10)$$

The bubble diameter (d_b) is calculated by [22] ;

$$d_b = 0.635\left(\frac{\sigma}{72}\right)^{0.6}\left(\frac{1}{\rho_L}\right)^{0.2} \qquad (11)$$

The liquid phase mass transfer coefficent (K_L) is calculated by [22] ;

$$K_L = \left(\frac{D_{CO_2}}{d_b}\right).\left(2 + 0.0187\left[\left(\frac{d_b U_g \rho_L}{\varepsilon_g \mu_L}\right)^{0.484}.\left(\frac{d_b g^{\frac{1}{3}}}{D_{CO_2}^{\frac{2}{3}}}\right)^{0.072}.\left(\frac{\mu_L}{D_{CO_2}\rho_L}\right)^{0.339}\right]^{1.61}\right) \qquad (12)$$

The Henry constant (H) is calculated by [15,23] ;

$$\log\left(\frac{H}{H_w}\right) = -\sum h_i\,.I \qquad (13)$$

$$\log(H_w) = \frac{1140}{T} - 5.3 \qquad (14)$$

Where: I=6.2

Enhancement factor (E) and the reaction rate constant (k) are calculated by [5] ;

$$E = \sqrt{1 + \frac{D_{CO_2} k}{K_L^{\,2}}} \qquad (15)$$

$$k = 2.2 * 10^{+7} * \left(\left[\exp\left(\frac{-71500}{R.T}\right)\right] - \left[3.2 * 10^{-6} * \rho_{H2O} * \exp\left(\frac{-13800}{R.T}\right)\right]\right) \qquad (16)$$

The CO_2 molecular diffusion coefficient (D_{CO2}) is calculated by [24] ;

$$D_{CO_2} = 5.35 * 10^{-10} * T * (\mu_L)^{-1.034} \qquad (17)$$

The pressure distribution and CO_2 partial pressure are calculated by;

$$P(z) = P_o - \left[\left(1 - \varepsilon_g\right).\rho_L.g.z\right] \qquad (18)$$

$$P_{CO_2}(z) = P(z)\ .y \qquad (19)$$

2.2 Mole Balance of liquid Phase (1st Section)

The overall mole balance of the liquid phase around the differential element with the absence of gas and solid phases (First Section) is:

$$\frac{dL}{dz} = 0 \qquad (20)$$

The mole balance equations for the dissolved species $NaHCO_3$, Na_2CO_3, and H_2O in liquid phase are:

$$\frac{d(L1)}{dz} = 2\,N_{CO_2}.\alpha_g \qquad (21)$$

$$\frac{d(L2)}{dz} = -N_{CO_2}.\alpha_g \qquad (22)$$

$$\frac{d(L3)}{dz} = -N_{CO_2}.\alpha_g \qquad (23)$$

2.3 Mole Balance of liquid Phase (2nd Section)

The overall mole balance of the liquid phase around the differential element in presence of solid phase (First Section) is:

$$\frac{dL}{dz} = -(2 + f).N_{CO_2}.\alpha_g \qquad (24)$$

ff is a factor which was found by trial and error to satisfy the supersaturation state which is an essential in all the precipitation of $NaHCO_3$ as shown in Fig. 2.

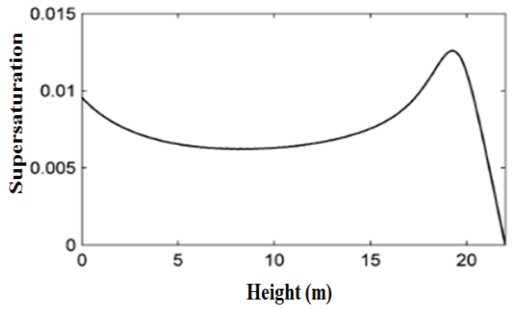

Fig. 2. Supersaturation vs. column length [17].

The mole balance equations for the dissolved species $NaHCO_3$, Na_2CO_3, and H_2O in liquid phase are:

$$\frac{d(L1)}{dz} = -f.N_{CO_2}.\alpha_g \quad (25)$$

$$\frac{d(L2)}{dz} = -N_{CO_2}.\alpha_g \quad (26)$$

$$\frac{d(L3)}{dz} = -N_{CO_2}.\alpha_g \quad (27)$$

2.4 Mole Balance of solid Phase and Crystallization

The mole balance for the solid ($NaHCO_3$) is:

$$\frac{dS}{dz} = (2+f).N_{CO_2}.\alpha_g \quad (28)$$

MATLAB program is used for solving Eqs. 7 to 28 and plotting figures.

Empirical power law equation for nucleation is used to find the primary number of crystals formed:

$$Bo = 26.685 * M_T^{0.42} * \Delta w^{1.31} \quad (29)$$

Solid product is divided into two unequal parts which was founded by trial and error. The biggest fraction (90%) of the solid production is contributed to the crystals growth and the small fraction (10%) is contributed to the crystals nucleation. Assume the part weight for nucleation and calculating the new crystals size that born , and then obtaining the growth part weight which from it calculating the crystals size growing and then checking the final crystals size in the outlet if satisfying the outlet weight by using the equation below:

$$Mass\ of\ Crystals = \sum_{1}^{Zi} Crystal\ volume(i) * Number\ of\ crystal(i) * \rho_{NaHCO_3} \quad (30)$$

Microsoft Excel program is used for crystallization calculation to obtain and plot the crystals size distribution (CSD) and cumulative mass fraction under size distribution. The values of the molar flux of $NaHCO_3$ crystals (S) were imported from the result of the MATLAB program as an arrow.

3. RESULTS AND DISCUSSION

3.1 Validation of the present Model

The present mathematical model work is validated with the previous work models. The CO_2 absorption efficiency of about 50% is found, in agreement with the two previous work groups [11, 18]. The comparison between the simulated solid productivity and magma density of the present work with the previous work [15] through the length of the column gives a good agreement is noticed (within 10% relative error), as shown in Figs. 3 and 4.

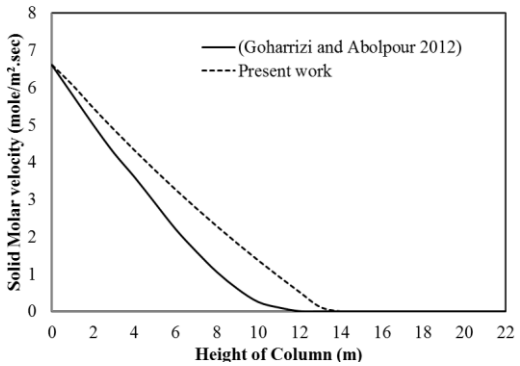

Fig. 3. A comparison between simulated solid phase distribution of the present work with the previous work through the length of column at conditions (G=15 mole/m^2.s, m_L=6800 kg/h, x_1=0.005, x_2=0.25, x_3=0.745, and y=0.56).

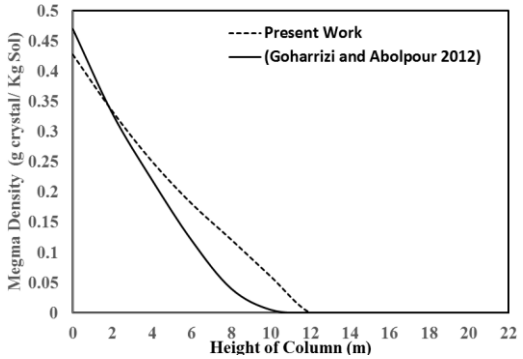

Fig. 4. A comparison between simulated magma density distribution of the present work and the previous work through the length of column at conditions (G=15 mole/m^2.s, m_L=6800 kg/h, x_1=0.005, x_2=0.25, x_3=0.745, and y=0.56).

3.3 Effect of process variables on $NaHCO_3$ production from flue gas

In this section the effect of process variables; gas molar velocity (G=2.5-10 mole/m^2.s), mass liquid flow rate (m_L=2800-3400 kg/h), sodium bicarbonate concentration (x_1=0.04-0.1), CO_2 gas mole fraction (y=0.02-0.18), column height(h=11-33 m), and column diameter(d_R=1-3 m) on the objective variables; solid molar velocity (S), CO_2 conversion, precipitation zone (Z_i), and crystal size distribution (CSD) were studied theoretically.

3.3.1 Effect of Gas molar velocity (G)

The effect of different gas molar velocities on the objective variables were studied while the other variables remained constants (m_L, y, x_1) as shown in Figs. 5 to 8. Fig. 5 illustrates the molar velocities distributions of gas, liquid, and solid phases through the length of the column., the liquid solution feed from the top of the column (at Z=22 m) to the first zone or supersaturation zone, and since there is no solid $NaHCO_3$ production in this zone and the molar velocity of the solid phase is zero therefore the changes in the liquid phase molar velocity in this zone is zero because of the amount of Na_2CO_3 + H_2O reactant

and the produced $NaHCO_3$ at the same quantity according to the stoichiometry of chemical reaction Eq. (6). The liquid phase molar velocity drops in precipitation zone after solid $NaHCO_3$ produced. Fig. 6 illustrates that the production of solid $NaHCO_3$ is increased from (0.3378 to 1.8167) $\frac{mol}{m^2.sec}$ mole/m^2.s with the increase of gas molar velocity from (2.5 to 10) mole/m^2.s. $\frac{mole}{m^2.sec}$ Increasing gas molar velocity lead to an increase in the gas velocity which raised the gas hold up according to Eq. 10 and increased the specific gas–liquid interfacial area according to Eq. 9 and also increased liquid phase mass transfer coefficient (K_L) according to Eq. 12, which in turn leads to an increase of the CO_2 flux (N_{CO2}) according to Eq. 8, and causes to increase in the solid production (S).

Fig. 7 shows that the conversion of CO_2 decrease from (58.6%5-51.7%) with increasing of the gas molar velocity from (2.5 to 10) mole/m^2.s $\frac{mole}{m^2.sec}$ because the high gas flow rate leads to high gas velocity, and that mean low residence time of CO_2 in the reactor leading to high outlet CO_2 gas mole fraction from column as shown in Fig. 8.

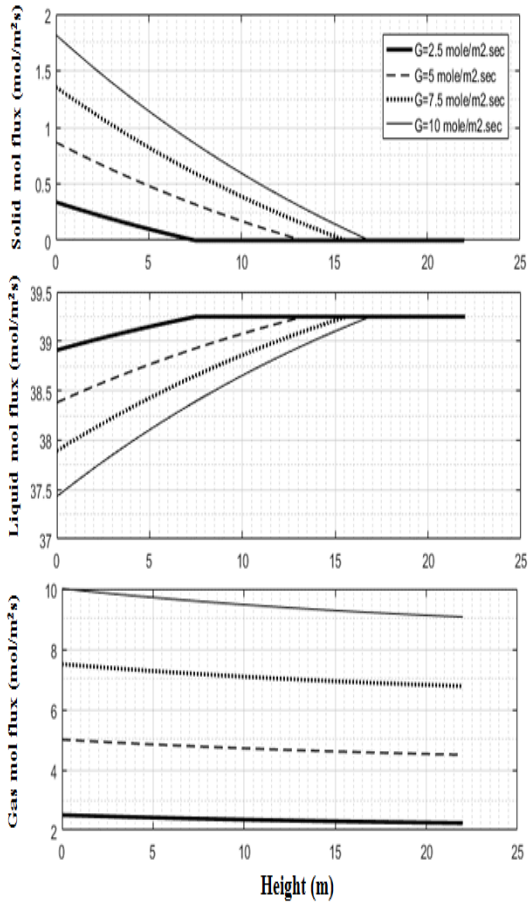

Fig. 5. Molar velocities distributions of three phases through the column at conditions: m_L=3500 kg/h, x_1=0.1, x_2=0.12, x_3=0.78, and y=0.18.

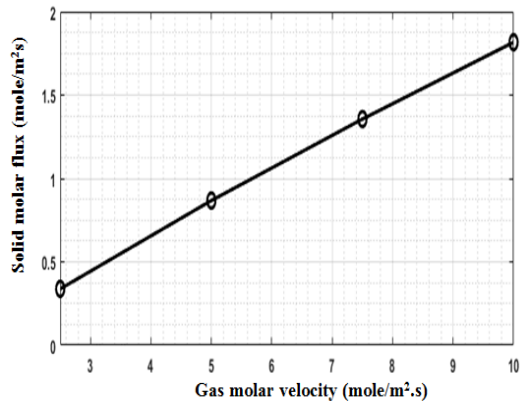

Fig. 6. $NaHCO_3$ production profile as a function of G at conditions: m_L=3500 kg/hr, x_1=0.1, x_2=0.12, x_3=0.78, and y=0.18

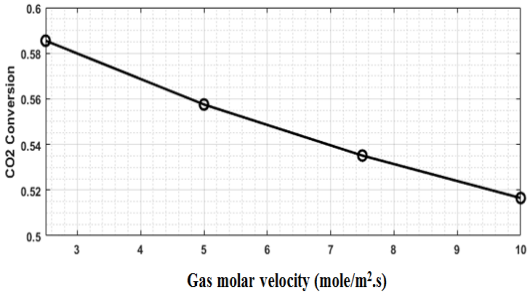

Fig. 7. CO_2 Conversion profile as a function of G at conditions: m_L=3500 kg/h, x_1=0.1, x_2=0.12, x_3=0.78, and y=0.18

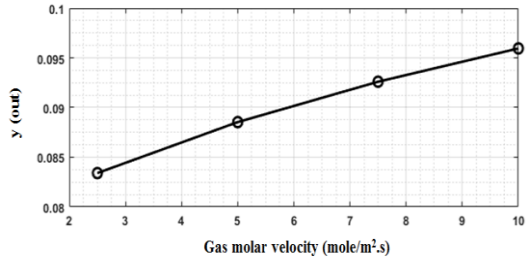

Fig. 8. Outlet CO_2 gas mole fraction at different G at conditions: m_L=3500 kg/h, x_1=0.1, x_2=0.12, x_3=0.78, and y=0.18

In Fig. 9, the precipitation zone (Z_i) is increased from (7.4-16.8) m with the increase of the gas molar velocity from (2.5 to 10) mole/m^2.s $\frac{mole}{m^2.sec}$ because of the high gas flow rate causes a higher input molar velocity of CO_2 which push the liquid solution to reach the maximum supersaturation at short supersaturation zone (Z-Z_i) from the enter point of the liquid solution and increased $NaHCO_3$ production(S).

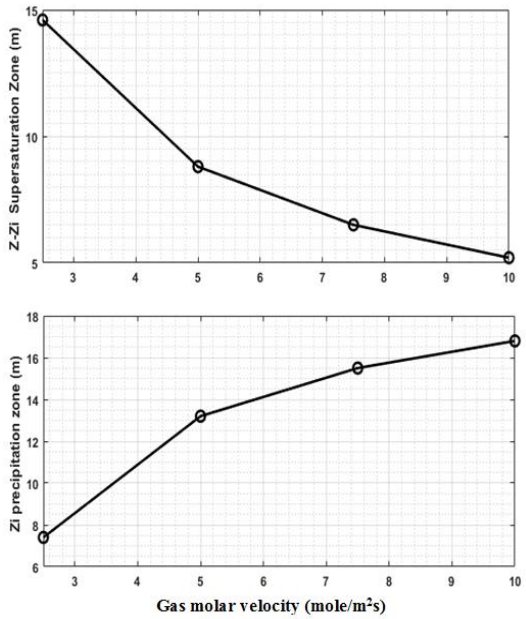

Fig. 9. Precipitation zone (Zi) and supersaturation zone (Z-Zi) as a function of at conditions: m_L=3500 kg/h, x_1=0.1, x_2=0.12, x_3=0.78, and y=0.18

Fig. 10 shows the cumulative mass fraction under size distribution at different gas molar velocities. A rise in crystal size was noticed when (G) increased from (2.5-10) $\frac{mole}{m^2.sec}$ mole/m^2.s. The increase in the gas molar velocity (G) can cause a rise in the precipitation zone (Zi) which raise the growth of crystals and causes the increase in the crystal size.

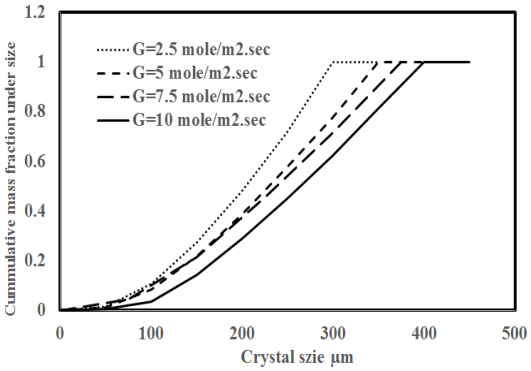

Fig. 10. Cumulative mass fraction under size distribution at different G at conditions: m_L=3500 kg/h, x_1=0.1, x_2=0.12, x_3=0.78, and y=0.18

3.3.2 Effects of CO_2 Gas Mole Fraction (y)

The effect of different CO_2 gas mole fraction from 0.02 to 0.18 on the objective variables were studied while the other variables are considered to be constants as shown in Figs. 11 to 14. Increasing the inlet CO_2 gas mole fraction from 0.02 to 0.18 rise the input molar velocity of CO_2 and thus more moles of CO_2 enter the column and that increasing the absorption efficiency from 0.5546 to 0.5575 as shown in Fig. 11. Increasing the CO_2 gas mole fraction from (0.02 to 0.18) lead to increase the production of solid $NaHCO_3$ (S) from (0.0927 to 1.0791) $\frac{mol}{m^2.sec}$ mole/m^2.s as shown in Fig. 12 due to increasing in the input CO_2 molar velocities.

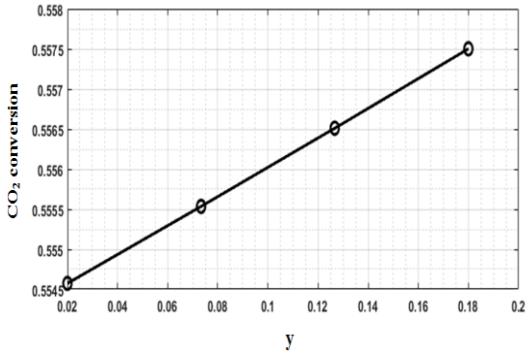

Fig. 11. CO_2 Conversion as a function of y at conditions: m_L=1000 kg/h, x_1=0.112, x_2=0.25, x_3=0.638, and G=5 mole/m^2.s

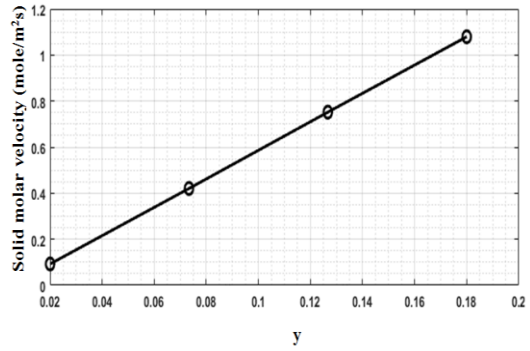

Fig. 12. Solid Production as a function of y at conditions: m_L=1000 kg/h, x_1=0.112, x_2=0.25, x_3=0.638, and G=5 mole/m^2.s

In Figs. 13 and 14, increasing the input CO_2 gas mole fraction (y) increased the precipitation zone (Z_i) from (10.2 - 20.2) m and decreased the supersaturation zone (Z-Z_i) from (11.80-1.8) m because in high CO_2 gas mole fraction more moles of CO_2 transferred from gas to liquid phase which drive the solution to reach the maximum supersaturation quickly and at small supersaturation zone.

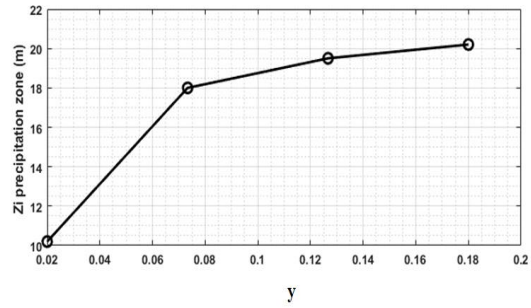

Fig. 13. Precipitation zone (Z_i) as a function of y at conditions: m_L=1000 kg/h, x_1=0.112, x_2=0.25, x_3=0.638, and G=5 mole/m^2.s

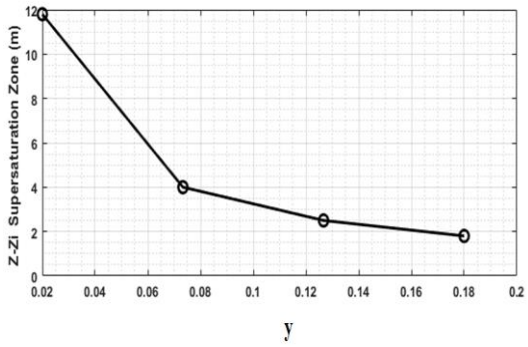

Fig. 14. Supersaturation zone ($Z-Z_i$) as a function of y at conditions: m_L=1000 kg/h, x_1=0.112, x_2=0.25, x_3=0.638, and G=5 mole/m^2.s

Fig. 15 shows the cumulative mass fraction under size distribution at different CO_2 gas mole fraction (y). An increase was noticed in the crystal size when (y) increased from (0.02-18). Increasing CO_2 gas mole fraction causes an increase in the precipitation zone (Zi) which causes an increase in the growth of the crystals which leads to rise crystal size.

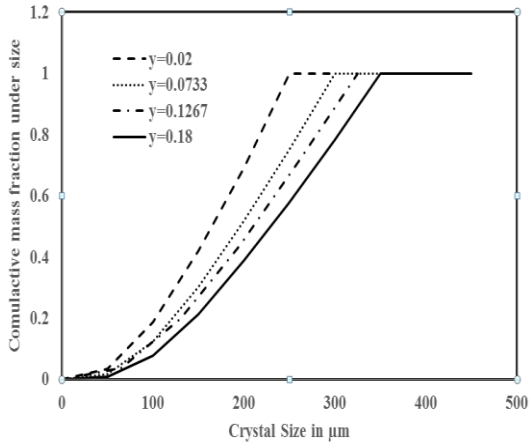

Fig. 15. Cumulative crystal size distribution at different y at conditions: m_L=1000 kg/h, x_1=0.112, x_2=0.25, x_3=0.638, and G=5 mole/m^2.s

3.3.3 Effect of Liquid Mass Flow rate (m_L)

The effect of different liquid mass flow rates (2800-3400 kg/h) on the objective variables were studied while the others variables are regarded to be constants (G, y, and x_1). Fig. 16 shows that the production of $NaHCO_3$ (S) was decreased from (0.7293 to 0.6458) mole/m2.s $\frac{mol}{m^2.sec}$ with the increase of the liquid mass flow rate (2800-3400 kg/h) because in low liquid mass flow rate small amount of CO_2 drives the liquid solution to reach maximum supersaturation quickly (in small supersaturation zone) and gave high solid productivity (S). Constant CO_2 conversion (0.5575) and constant outlet CO_2 gas mole fraction (0.0885) is noticed with the change in the liquid mass flow rate because CO_2 absorption rate is independent in liquid mass flow rate.

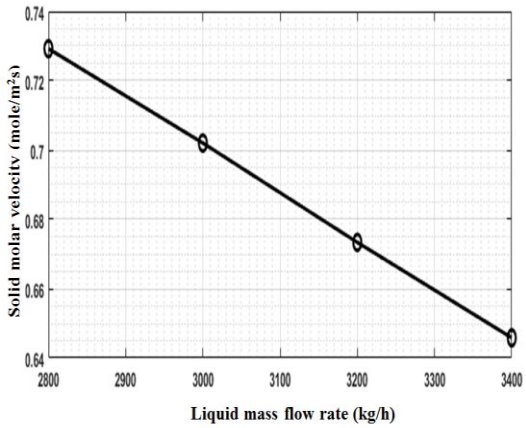

Fig. 16. Solid Production(S) as a function of liquid mass flow rate (m_L) and constant conditions: G=5 mole/m^2.s, x_1=0.08, x_2=0.1, x_3=0.82, y=0.18

The precipitation zone (Zi) was decreased from (10.5-8.7) m with increasing liquid mass flow rate (2800-3400 kg/h) because of high liquid mass flow rate needs a larger supersaturation zone ($Z-Z_i$) to reach the maximum supersaturation state as shown in Figs. 17 and 18.

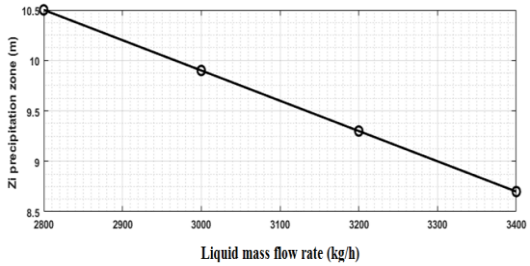

Fig. 17. Precipitation zone (Zi) as a function of liquid mass flow rate (m_L) and constant conditions: G=5 mole/m^2.s, x_1=0.08, x_2=0.1, x_3=0.82, y=0.18

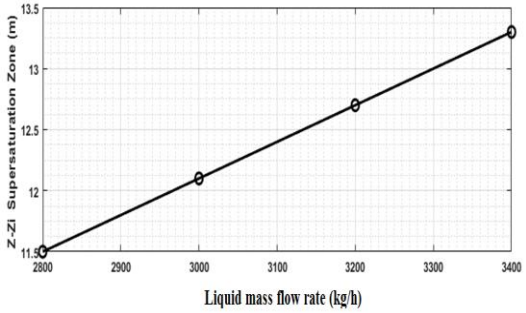

Fig. 18. Supersaturation zone (Z-Zi) as a function of liquid mass flow rate (m_L) and constant conditions: G=5 mole/m^2.s, x_1=0.08, x_2=0.1, x_3=0.82, y=0.18

Fig. 19 shows the cumulative mass fraction under size distribution at different liquid mass flow rates (m_L). A decrease was noticed in the crystal size when (m_L) increased from (2800-3400 kg/h). Increasing the liquid mass flow rate caused a decrease in the precipitation zone (Zi) which reduce the growth of crystals and causes a reduction in crystals size.

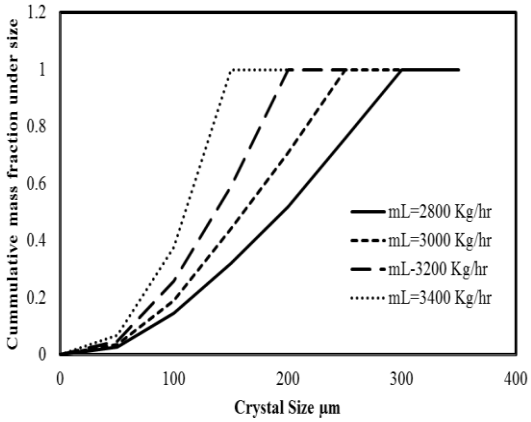

Fig. 19. Cumulative mass fraction under size distribution at different (m_L) and constant conditions: G=5 mole/m^2.s, x_1=0.08, x_2=0.1, x_3=0.82, y=0.18

3.3.4 Effect of $NaHCO_3$ concentration (x_1)

The effect of different $NaHCO_3$ concentration (x_1) from (0.04-0.1) on the objective variables were studied while the other operation variables seem to be constant as shown in Figs. 20 and 21.

In Fig. 20 the production of solid $NaHCO_3$ increased from (0.4629-0.9445) mole/m^2.s $\frac{mol}{m^2.sec}$ with the increase of sodium bicarbonate (x_1) from (0.04-0.1) because at low concentration of sodium bicarbonate (x_1) an amount of CO_2 drives the liquid solution to reach maximum supersaturation slowly (in large supersaturation zone) yield low solid productivity (S).

Constant CO_2 conversion (0.5575) and constant outlet CO_2 gas mole fraction (0.0885) is noticed with the change in (x_1) because CO_2 absorption rate is independent in $NaHCO_3$ concentration (x_1).

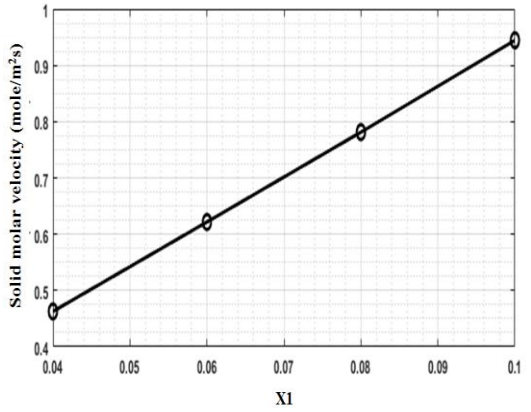

Fig. 20. Solid Production(S) as a function of x_1 and constant conditions: G=mole/m^2.s, x_2=0.1, y=0.18, m_L=2400 kg/h

In Fig. 21 the precipitation zone (Zi) is increased from (5.8-15.5) m with the increase of (x_1) because when (x_1) is a high value then the liquid solution reach the maximum supersaturation in small supersaturation zone(Z-Zi) and the longist distance of column was used for precipitation.

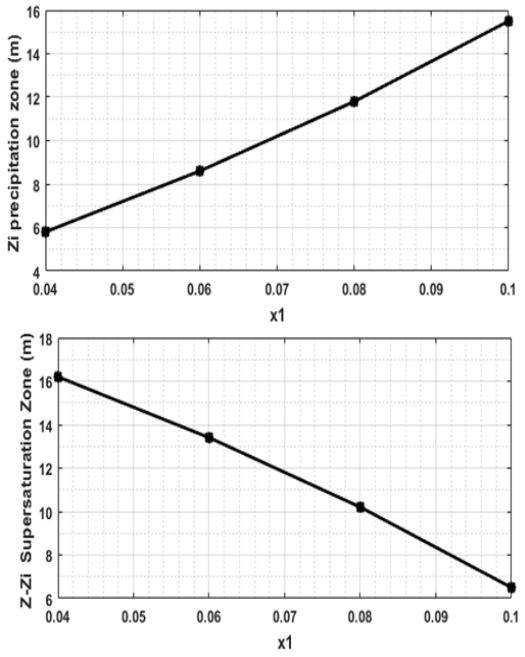

Fig. 21. Precipitation zone (Zi) and supersaturation zone (Z-Zi) at different $NaHCO_3$ concentrations (x_1) and constant conditions: G=mole/m^2.s, x_2=0.1, y=0.18, m_L=2400 kg/h

Fig. 22 shows the cumulative mass fraction under size distribution at different sodium bicarbonate concentrations (x_1). A crystal size grow was noticed when (x_1) is raised. The rising in the concentration of sodium bicarbonate (x_1) causes an elevated precipitation zone (Zi), which lead to an increase in the crystals growth and crystals size.

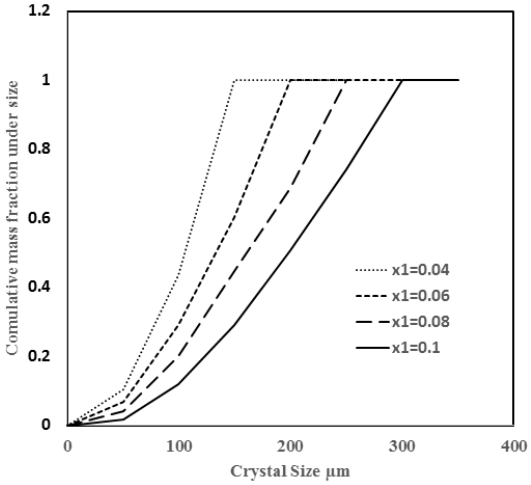

Fig. 22. Cumulative crystal size distribution at different $NaHCO_3$ concentrations (x_1) constant conditions: G=5mole/m^2.s, x_2=0.1, y=0.18, m_L=2400 kg/h

3.3.5 Effects of column height

The effect of rising (h) from (11-33) m on the productivity and CO_2 conversion and precipitation zone were studied at a specific conditions (G=7.5 mole/m^2.s, m_L=4200 kg/h, x_1=0.1, x_2=0.12, x_3=0.78, and y=0.18) as shown in Figs. 23 to 26. Fig. 23 illustrates that the production of $NaHCO_3$ is increased with the rising of (h) which drives to increase the residence time of CO_2 in the column, and that causes an improvement in the absorption and conversion of CO_2 as shown in Fig. 24 and that leads

to producing more of $NaHCO_3$ in the column. Fig. 25 shows a direct correlation between the height of the column (h) and the precipitation zone because that the small height mean low residence time of CO_2 which mean small amount of molar velocity of absorbed CO_2 to reach the solution to the supersaturation state which means large supersaturation zone (Z-Zi).

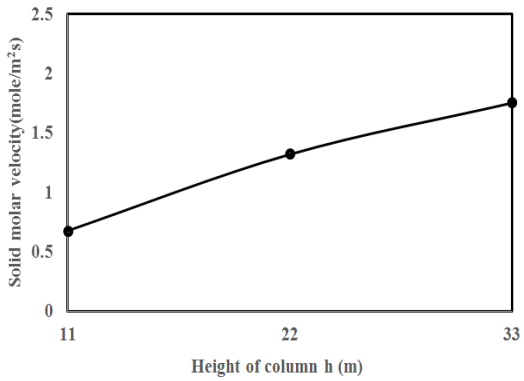

Fig. 23. Effects of h on S at conditions G=7.5 mole/m^2.s, m_L=4200 kg/hr, x_1=0.1, x_2=0.12, x_3=0.78, and y=0.18).

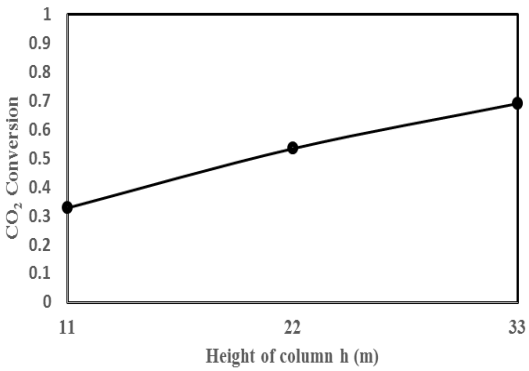

Fig. 24. Effects of h on CO_2 conversion at conditions G=7.5 mole/m^2.s, m_L=4200 kg/h, x_1=0.1, x_2=0.12, x_3=0.78, and y=0.18).

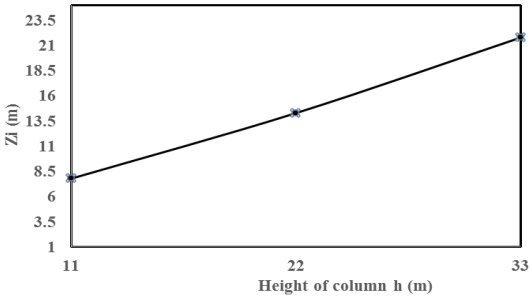

Fig. 25. Effects of h on Z_i at conditions G=7.5 mole/m^2.s, m_L=4200 kg/h, x_1=0.1, x_2=0.12, x_3=0.78, and y=0.18).

Fig. 26 shows a positive correlation between the cumulative mass fraction under size distribution and the column height (h). A rise in the crystals size was noticed when (h) is raised which causes an enlargement in the precipitation zone (Zi) and that drives crystals size to growth.

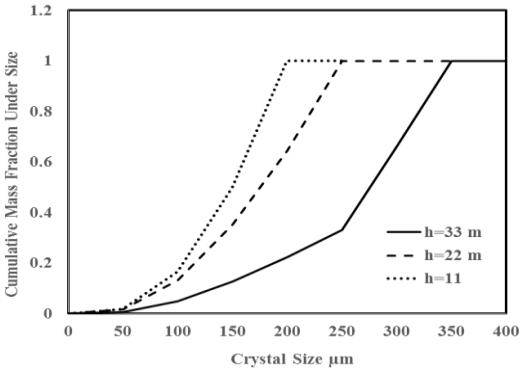

Fig. 26. Cumulative mass fraction under size at the bottom of column at different (h)

3.3.6 Effects of column diameter

An approximate estimation for the production of $NaHCO_3$ as a function of the column diameter is calculated using a typical design value of molar gas flux G=5 mole/m^2.sec. The effect of column diameter on productivity is illustrated in Fig. 27, which increased with the increase of the column diameter.

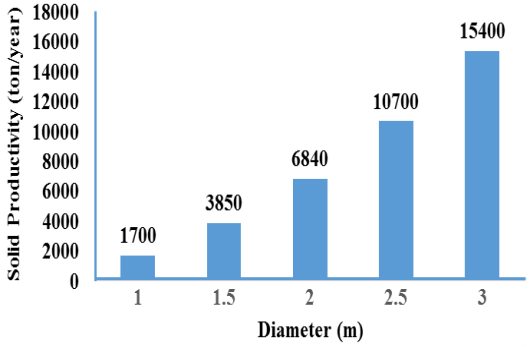

Fig. 27. Effects of column diameter on productivity at conditions: G=5 mole/m^2.s, m_L=3500 kg/h, x_1=0.1, x_2=0.12, x_3=0.78, and y=0.18.

4. CONCLUSIONS

1- A rising in sodium bicarbonate production was noticed with the rising in gas molar velocity (G), CO_2 gas mole fraction (y), sodium bicarbonate concentration (x_1), height of column (h), and diameter of column (d_R). Whereas it reduced with the rising of the liquid mass flow rate (m_L).

2- The conversion of CO_2 improved with the increase of CO_2 gas mole fraction (y) and the column height (h) and dropped with the increase of gas molar velocity (G), whereas it was not effected by the change of the liquid mass flow rate (m_L) and sodium bicarbonate concentration (x_1).

3- Enlargement in the precipitation zone (Z_i) was noticed with the increase of gas molar velocity (G), CO_2 gas mole fraction (y), sodium bicarbonate concentration (x_1), and height of column (h). Whereas decreased with the increase of liquid mass flow rate (m_L).

4- A positive association was noticed between the particle size and the gas molar velocity (G), CO_2 gas mole fraction (y), sodium bicarbonate concentration (x_1), and the height of column (h). While was an inverse relationship with the liquid mass flow rate (m_L) and the particle size range varies from 0 to 400 µm.

NOMENCLATURES

A	Column cross section area	m^2
b	Order of nucleation	-
Bo	Nucleation rate	No.s-1(kg solution)-1
D_{AB}	Molecular diffusion coefficient of Substance A	$m^2.s^{-1}$
d_b	Bubble diameter	m
D_{CO2}	Molecular diffusion coefficient of CO_2	$m^2.s^{-1}$
D_g	Gas Axial Dispersion	$m^2.s^{-1}$
D_L D_L D_L	Liquid Axial Dispersion	$m^2.s^{-1}$
d_R	Column diameter	m
E	Enhancement Factor	-
f	Factor find by trial and error to satisfy the supersaturation	-
g	Gravitational constant	$m.s^2$
G	Molar velocity (flux) of gas	$Mole\ m^{-2}.s^{-1}$
G_1	Molar velocity of CO_2 gas	$mole.m^2s^{-1}$
gc	Growth order	-
G_o	Growth rate	$\mu m.sec^{-1}$
h	Height of Column	m
H	Henry constant	$Kmol.atm^{-1}.m^{-3}$
h_i	Salting out parameter for each electrolyte	$m^3.Kmole^{-1}$
H_w	Henry constant of water	$Kmol.atm^{-1}m^{-3}$
I_i	Ionic strength for each electrolyte	$Kmole.m^{-3}$
j	Order of magma density	-
k	Constant rate reaction	s^{-1}
k_g	Growth rate constant	-
K_L	Liquid phase mass transfer coefficient	$m.s^{-1}$
K_N	Nucleation rate constant	-
L	Molar liquid velocity(flux)	$mole.m^{-2}s^{-1}$
m_L	Liquid mass flow rate	$kg.h^{-1}$
M_T	Magma density	$g_{crys}.kg_{sol}^{-1}$
N_{CO2}	CO_2 Flux of mass transfer	$mole.m^{-2}.s^{-1}$
$P_{CO2(e)}$	CO_2 partial pressure at bulk liquid phase	atm
$P_{CO2}(z)$	CO_2 partial pressure at interface through the column	atm
Q_g	Volumetric Gas Flow rate	$Nm^3.h^{-1}$
R	Gases constant	$J(mole\ K)^{-1}$
S	Molar Solid velocity (flux)	$mole.m^{-2}.s^{-1}$
T	Temperature	K
U_b	Bubble rising velocity	$m.s^{-1}$
U_g	Superficial velocity of gas	$m.s^{-1}$
U_L	Liquid velocity	$m.s^{-1}$
x*	Mole fraction of $NaHCO_3$ at supersaturation	-
x_1	Mass fraction of $NaHCO_3$	-
X_1	Mole fraction of $NaHCO_3$	
x_2	Mass fraction of Na_2CO_3	-
X_2	Mole fraction of Na_2CO_3	
x_3	Mass fraction of H_2O	-
X_3	Mole fraction of H_2O	-
y	CO_2 gas fraction	-
z	Height of Column	m
Z_i	Height of column that sodium bicarb reaches to sat. conc.	m

Greek Symbols

μ_l	Liquid dynamic viscosity	$N.sec.m^{-2}$
α_g	Gas-liquid interface	$m^2.m^{-3}$
ε_g	Gas holdup	-
ε_l	Liquid holdup	-
ρ_{H2O}	Water density	$kg.m^{-3}$
ρ_l	Liquid density	$kg.m^{-3}$
σ_l	Liquid surface tension	$N.m^{-1}$
υ_l	Liquid kinematic viscosity	$m^2.sec^{-1}$
Δw	Supersaturation	$g_{NaHCO3}.(kg_{sol})^{-1}$

REFERENCES

[1] Song C, Gaffney AF, Fujimoto K. CO_2 conversion and utilization, American Chem. Soci 2002.

[2] Abdel-Rahman ZA, Hamed HH, Khalaf FK. Optimization of Sodium Bicarbonate Production Using Response Surface Methodology (RSM), Diyala J. of Eng. Sci. 2018;11(3) 22- 28.

[3] Hikita H, Asai S, Takatsuka T. Absorption of carbon dioxide into aqueous sodium hydroxide and sodium carbonate- bicarbonate solutions. The Chemical Engineering Journal 1976; 11(2): 131-141.

[4] Salehi K, Jokar SM, Shariati J, Bahmani M, Sedghamiz MA, Rahimpour MR. Enhancement of CO conversion in a novel slurry bubble column reactor for methanol synthesis. J. of Natural Gas Science and Engineering 2014; 21: 170-183.

[5] Saberi A, Goharrizi AS, Ghader S. Precipitation kinetics of sodium bicarbonate in an industrial bubble column crystallizer. Crystal Research and Technology. Journal of Experimental and Industrial Crystallography 2009; 44(2): 159-166.

[6] Mersmann, A., Crystallization technology, 1995.

[7] Balasko B, Nemeth S, Janecska A, Nagy T, Nagy G, Abonyi J. Process modeling and simulation for optimization of operating processes. In V. Pleşu & P. Ş. Agachi (Eds.). Computer Aided Chemical Engineering 2007; (24): 895.

[8] Jung S, Becker M, Agar DW, Franke R. One-Dimensional Modeling and Simulation of Bubble Column Reactors. Chemical Engineering & Technology 2010; 33(12): 2037-2043.

[9] Haut Bt, Cartage T. Mathematical modeling of gas–liquid mass transfer rate in bubble columns operated in the heterogeneous regime. Chem. Eng. Sci. 2005; 60(22): 5937-5944.

[10] Haut BT, Halloin V, Cartage T, Cockx A. Production of sodium bicarbonate in industrial bubble columns. Chem. Eng. Sci 2004; 59(22-23):5687-5694.

[11] Wylock CE, Colinet P, Cartage T, Haut B. Coupling between mass transfer and chemical reactions during the absorption of CO_2 in a $NaHCO_3$-Na_2CO_3 brine: experimental and theoretical study. International J. of Chemical Reactor Engineering 2008; 6(1).

[12] Wylock CE, Larcy A, Colinet P, Cartage T, Haut B. Study of the CO_2 Transfer Rate in a Reacting Flow for the Refined Sodium Bicarbonate Production Process. Proceedings of the COMSOL Conference, Hannover 2008.

[13] Wylock CE, Larcy A, Cartage T, Haut B. Compartmental modeling of an industrial column. Chem.Product and Proc. Modeling 2009; 4(5).

[14] Wylock CE, Gutierrez V, Debast F, Delplancke-Ogletree MP, Cartage T, Haut B. Influence of mixing and solid concentration on sodium bicarbonate secondary nucleation rate in stirred tank: theoretical and experimental studies. Crystal Research and Technology 2010; 45 (9): 929-938.

[15] Goharrizi AS, Abolpour B. Estimation of sodium bicarbonate crystal size distributions in a steady-state bubble column reactor. Research on Chemical Intermediates 2012; 38(7): 1389-1401.

[16] Goharrizi RS, Abolpour B. Estimation of nucleation and growth rate of sodium bicarbonate crystals in a steady-state bubble column reactor. Research on Chemical Intermediates 2013; 41(3): 1459-1471.

[17] Goharrizi AS, Abolpour B. Modeling an industrial sodium bicarbonate bubble column reactor. Applied Petrochemical Res 2014; 4(2): 235

[18] Maharloo DG, Darvishi A, Davand R, Saidi M, Rahimpour MR. Process intensification and environmental consideration of sodium bicarbonate production in an industrial soda ash bubble column reactor by CO_2 recycling. Journal of CO_2 Utilization 2017; 20, 318.

[19] Wylock CE, Rednikov A, Colinet P, Haut B. Experimental and numerical analysis of buoyancy-induced instability during CO_2 absorption in $NaHCO_3$–Na_2CO_3 aqueous solutions. 2017; 157: 232-246.

[20] Danckwerts PV, Lannus A. Gas-liquid reactions. Journal of the Electrochemical Society 1970; 117(10): 369C-370C.

[21] Kantarci N, Borak F, Ulgen KO. Bubble column reactors. Proc. Biochem. 2005; 40(7): 2263.

[22] Hughmark GA. Holdup and Mass Transfer in Bubble Columns. Indust. & Eng. Chemistry Process Design and Development 1967; 6(2): 218-220.

[23] Pohorecki R, Moniuk WDW. Kinetics of reaction between carbon dioxide and hydroxyl ions in aqueous electrolyte solutions. Chemical engineering science 1988; 43(7): 1677-1684.

[24] Tamimi A, Rinker EB, Sandall OC. Diffusion coefficients for hydrogen sulfide, carbon dioxide, and nitrous oxide in water over the temperature range 293-368 K. Journal of Chemical and Engineering data 1994; 39(2): 330-332.